Molecular Therapy
Nucleic Acids
Original Article

Müller glia-derived exosomal miR-9-3p promotes angiogenesis by restricting sphingosine-1-phosphate receptor $S1P_1$ in diabetic retinopathy

Yu Liu,[1,3] Qin Yang,[1,3] Haixin Fu,[2] Jingfan Wang,[1] Songtao Yuan,[1] Xinsheng Li,[1] Ping Xie,[1] Zizhong Hu,[1] and Qinghuai Liu[1]

[1]Department of Ophthalmology, The First Affiliated Hospital of Nanjing Medical University, Nanjing 210029, China; [2]Department of Ophthalmology, The Huai'an Hospital of Huai'an City, Huai'an 223200, China

Diabetic retinopathy is a heterogeneous retinal degenerative disease with the microvascular dysfunction being recognized as a hallmark of the advanced stage. In this study, we demonstrated that exosomes collected from the vitreous humor of proliferative diabetic retinopathy patients promoted proliferation, migration and tube formation ability of primary human retinal endothelial cells via its elevated miR-9-3p expression level. Müller glia cells were further recognized as the sole source of the aberrantly expressed miR-9-3p, and both *in vitro* and *in vivo* experiments validated that Müller glia-derived exosomes aggravate vascular dysfunction under high glucose. Mechanistically, exosomal miRNA-9-3p was transferred to retinal endothelial cells and bound to the sphingosine-1-phosphate receptor $S1P_1$ coding sequence, which subsequently activated VEGFR2 phosphorylation and internalization in the presence or absence of exogenous VEGF-A. We successfully orchestrated the dynamic crosstalk between retinal Müller glia cells and endothelial cells in pathological condition, which may provide a novel biomarker or promising therapeutic agents for the treatment of diabetic retinopathy.

INTRODUCTION

Diabetic retinopathy (DR) is a leading cause of visual impairment among working-age adults worldwide.[1,2] In the advanced stage of DR, abnormal formation of new blood vessels, resulting from progressive dysfunction of retinal endothelial cells is recognized as the major pathological change.[3–5] However, present treatment, including laser photocoagulation, intravitreal injection of anti-vascular endothelial growth factor (VEGF) drugs, or vitreoretinal surgery can only restore and maintain part of the vision, making early control of abnormal angiogenesis desperately needed for the treatment of DR.[6–9]

It has long been known that DR is a complex and heterogeneous retinal degenerative disease with all components of the retina being disrupted in disease progression.[10] The term, "neurovascular unit," was first introduced to emphasize the intimate relationship between the brain and its vessels.[11,12] As part of the central nervous system, the retina is composed of neurons, glia cells, endothelial cells, pericytes, and extracellular matrix components.[13,14] Deeper understanding of the cellular and molecular changes of retinal neurovascular unit in DR is important for future preventative and therapeutic strategies for DR.

During the past decade, exosome, as a class of extracellular vehicles (30–150 nm diameter), has been indicated to play important roles in intercellular communication.[15–17] Most cells can secrete exosomes, which can then be internalized by recipient cells,[18] participating in variable biological processes.[19,20] Unlike other extracellular fluids, such as blood, urine, and ascitic fluid, the human vitreous is relatively small in volume (around 4.5 mL) and difficult to obtain, making studies reported in the context of vitreal exosomes mediating retinal neurovascular interaction rare.[21]

In this study, we demonstrated that exosomes collected from surgically obtained vitreous humor of patients with proliferative diabetic retinopathy (PDR) promote cell proliferation, migration, and tube formation of primarily cultured human retinal endothelial cells (hRECs), and thus result in retinal hypervascularization. Exosomal miRNA-9-3p (miR-9-3p) was further identified as the key mediator participating in Müller glia (MGs)-induced endothelial dysfunction both *in vivo* and *in vitro*. Furthermore, we demonstrate that miR-9-3p promoted angiogenesis by targeting $S1P_1$ and $S1P_1$ overexpression blocks VEGF-A induced VEGFR2

Received 8 March 2021; accepted 15 December 2021;
https://doi.org/10.1016/j.omtn.2021.12.019.

[3]These authors contributed equally

Correspondence: Ping Xie, Department of Ophthalmology, The First Affiliated Hospital of Nanjing Medical University, 300 Guangzhou Road, Nanjing 210029, China.
E-mail: xieping9@126.com
Correspondence: Zizhong Hu, Department of Ophthalmology, The First Affiliated Hospital of Nanjing Medical University, 300 Guangzhou Road, Nanjing 210029, China.
E-mail: huzizhong@njmu.edu.cn
Correspondence: Qinghuai Liu, Department of Ophthalmology, The First Affiliated Hospital of Nanjing Medical University, 300 Guangzhou Road, Nanjing 210029, China.
E-mail: liuqh@njmu.edu.cn

phosphorylation and vascular sprouting in hRECs. Taken together, our study successfully delineated the role of aberrantly regulated exosomal miRNA in DR pathology and provided potential targets for developing novel therapeutic interventions for DR.

RESULTS

Proangiogenic effects of exosomes derived from vitreous humor of PDR patients

Vitreal exosomes from 65 PDR patients and 63 sex- and age-matched macular hole (MH) patients were isolated and characterized for the exosomal markers (TSG 101, CD63, CD81, and Calnexin) by Western blot as shown in Figure 1B.[22] Transmission electron microscopy was used to reveal the characteristic sizes and shapes of exosomes (Figure 1C). PDR-exo as well as MH-exo, pre-incubated with PKH dye, were found to have been taken up by hRECs (Figure 1D).[23] The concentration of exosomal proteins was quantified by the BCA method (Figure S1), according to which two groups of exosomes were incubated with hRECs for 48 h with a final concentration of 100 μg/mL. Compared with PBS and MH-exo, PDR-exo promoted cell proliferation and viability of hRECs, as demonstrated by EdU assay and cck8 assay ($p < 0.05$, Figure 1F). Also, PDR-exo-treated hRECs showed enhanced migration, and tube-forming ability ($p < 0.05$, Figures 1G and 1H).

MiR-9-3p as the key proangiogenic component in exosomes derived from vitreous humor of PDR patients

To define the specific exosomal miRNA that participates in angiogenesis, we compared the expression profiles of miRNAs by microarray analysis between PDR-exo and MH-exo. A total of 434 aberrantly expressed miRNAs, among which 82 upregulated miRNAs were screened in PDR-exo (false discovery rate < 0.05, fold change >2) (Figures 2A and S2A). After qRT-PCR validation of the top 5 upregulated miRNAs, miR-9-3p stood out as the most significantly upregulated in PDR-exo (Figure S2B). Considering that multiple studies have reported on the important roles of miR-9-3p in modulation of angiogenesis (Figure S2C),[24–27] we hypothesized that PDR-exo may participate in the pathological angiogenesis via its elevated miR-9-3p level.

qRT-PCR also validated that miR-9-3p level in hRECs was significantly upregulated after PDR-exo treatment for 48 h. To explore the key component that regulates the hREC's functions, 50 nM miR-9-3p inhibitor was transfected in hRECs and proved to downregulate the miR-9-3p expression level by approximately 70% ($p < 0.05$, Figure 2B). Meanwhile, the miR-9-3p inhibitor neutralized the proangiogenic effects of the PDR-exo by suppressing proliferation, migration, and tube-forming ability in hRECs ($p < 0.05$, Figures 2C–2E). Collectively, these results suggested that miR-9-3p may be essential for PDR-exo to promote pathological angiogenesis.

$S1P_1$ was identified as the key component of miR-9-3p to regulate abnormal angiogenesis

To investigate how miR-9-3p promotes the angiogenesis, the potential targets of miR-9-3p were predicted using five public databases (miRDB, TargetScan, microT, miRmap, and Starbase), among which, $S1P_1$, a receptor for the blood-borne bioactive lipid sphingosine-1-phosphate S1P, was identified as the target of miR-9-3p and was reported to stabilize VEGFR2 activation in endothelial cell lines[28,29] (Figure 3A). Co-transfecting miR-9-3p with 3′ UTR-$S1P_1$-WT vectors significantly decreased the luciferase activity, while there was no effect after co-transfection of miR-9-3p with 3′ UTR-$S1P_1$-MUT or blank vector in HEK293T ($p > 0.05$, Figure 3B). We further conducted $S1P_1$, in conjunction with CD31 (endothelial marker), immunostaining in the proliferative membrane (harvested in vitreoretinal surgery) and found that $S1P_1$ is detectable in human vessels (Figure 3C). Consistent with the previous report that $S1P_1$ regulates the angiogenetic process by regulating VEGFR2 phosphorylation,[25] Kyoto Encyclopedia of Genes and Genomes screening of our miRNA sequencing also indicated that AKT phosphorylation signaling was activated in the vitreous humor of PDR patients (Figure 3D). We hypothesized that $S1P_1$ may play a key role in vascular stabilization by regulating the VEGFR2 phosphorylation process. Both $S1P_1$ overexpression and SU5416 administration alleviated the enhanced cell proliferation, migration, and tube formation caused by miR-9-3p (Figures 3E–3G).[30] Taken together, our results showed that the pro-angiogenic effects of miR-9-3p were largely reversed by $S1P_1$ overexpression, indicating that $S1P_1$ may be the key downstream molecule of miR-9-3p. Also, observed phenotypic similarities between $S1P_1$ overexpression and SU5416 treatment imply that $S1P_1$ may exert its role by mediating the VEGFR2 phosphorylation process.

$S1P_1$ depletion accelerates endogenous and exogenous VEGF-A-induced VEGFR2 phosphorylation and internalization

To study the effect of $S1P_1$ activity on VEGFR2 signaling *in vitro*, miR-9-3p mimics as well as $S1P_1$ plasmid were transfected in hRECs. Western blotting results showed that phosphorylation of AKT, ERK, and VEGFR2 were notably promoted by miR-9-3p mimics and blocked when $S1P_1$ was overexpressed. Also, we pretreated hRECs with sFlt1 to block the endogenous VEGF signaling and stimulated hRECs with 50 ng/mL VEGF-A for 15 min.[31,32] As shown in Figure 4A, exogenous VEGF-A stimulation brought rapid phosphorylation of AKT, ERK, and VEGFR2, which was augmented by miR-9-3p mimics and partially abolished in the $S1P_1$ OE group.

Furthermore, we noticed that miR-9-3p mimics caused enhanced VEGFR2 internalization in the presence or absence of exogenous VEGF-A stimulation, while the $S1P_1$ OE group exhibited impaired VEGF-A-induced endocytosis as reflected by decreased colocalization with EEA1, an endosomal marker (Figure 4B).[33–35] Collectively, these data show that $S1P_1$ influences both endogenous and exogenous VEGF-A-induced VEGFR2 phosphorylation *in vitro* by inhibiting the AKT/ERK signaling pathway.

High glucose cultured hMGs are identified as the source of elevated exosomal miR-9-3p

We explored the expression pattern of miR-9-3p in multiple retinal cell types, including hRECs, hMGs, human retinal pigment epithelial cells (ARPE19), and human micro glia cell line (hMC3), and their

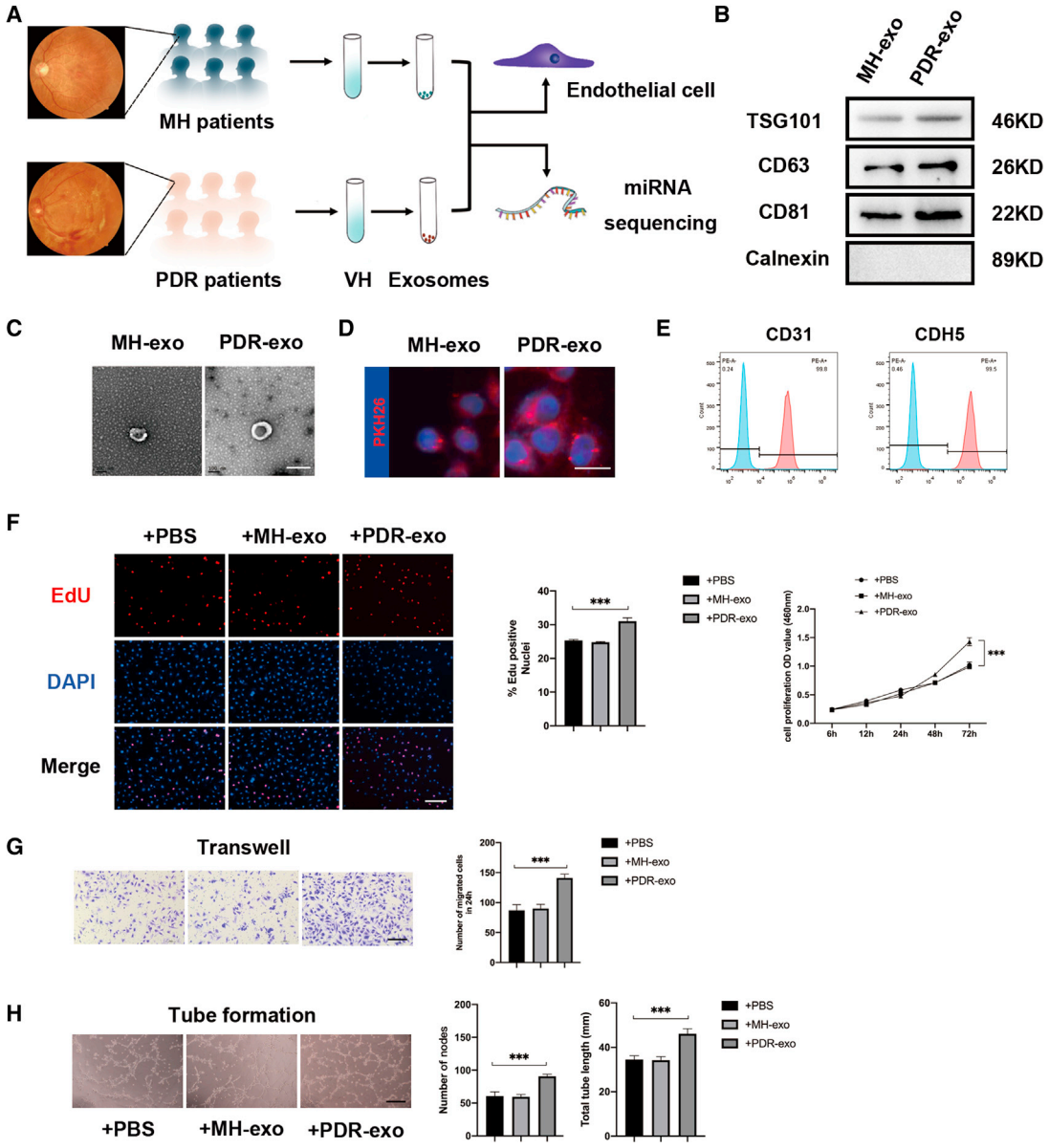

Figure 1. Characterization of exosomes from PDR and MH patients and identification of their effects on hRECs

(A) Schematic diagram showing that exosomes were extracted from the vitreous humor of PDR and MH patients for subsequent experiments. Panels of eye fundus images are presented to show the abnormal angiogenesis of PDR patients. (B) Representative bands showing exosomal surface marker protein expression levels of TSG101, CD63, CD81, and Calnexin. (C) Representative micrographs showing exosome ultrastructure. Scale bar, 100 nm.(D) Uptake of exosomes by hRECs was detected by PKH26. Exosomes labeled with PKH26 are stained red, while the nuclei of hRECs are stained blue. Scale bar, 20 μm. (E) Flow cytometric analysis of characteristic cell markers of endothelial cells. Blue curves represent isotype controls for PE dye and red curves represent measured markers (CD31 and CDH5, respectively). This experiment was repeated triplicate independently. (F–H) Following coincubation with 100 μg/mL PDR-exo for 48 h, cell proliferation, migration, and tube formation ability of hRECs were assessed. (F) hRECs viability measured by cck8 assay and cell proliferation measured by EdU assay. The percentage of EdU-positive cells (labeled red) was calculated in three randomly selected fields. Scale bar, 100 μm. (G) Migration of hRECs determined by transwell assay. Scale bar, 100 μm. (H) Tube formation ability was measured. Scale bar, 100 μm. EdU, transwell, and tube formation assay were conducted three independent times and each group included three replicas. For cck8 assay, three independent experiments as well as five replicas were conducted. Mean ± SEM are provided and ***$p < 0.001$.

respective exosomes, under low and high glucose to investigate which specific retinal cell type generated the abnormal upregulated exosomal miR-9-3p. qRT-PCR results showed that miR-9-3p expression level was solely increased in hMGs as well as in its derived exosomes under high glucose (Figures 5A and S3A). Moreover, nanoparticle tracking analysis confirmed that there was no difference between

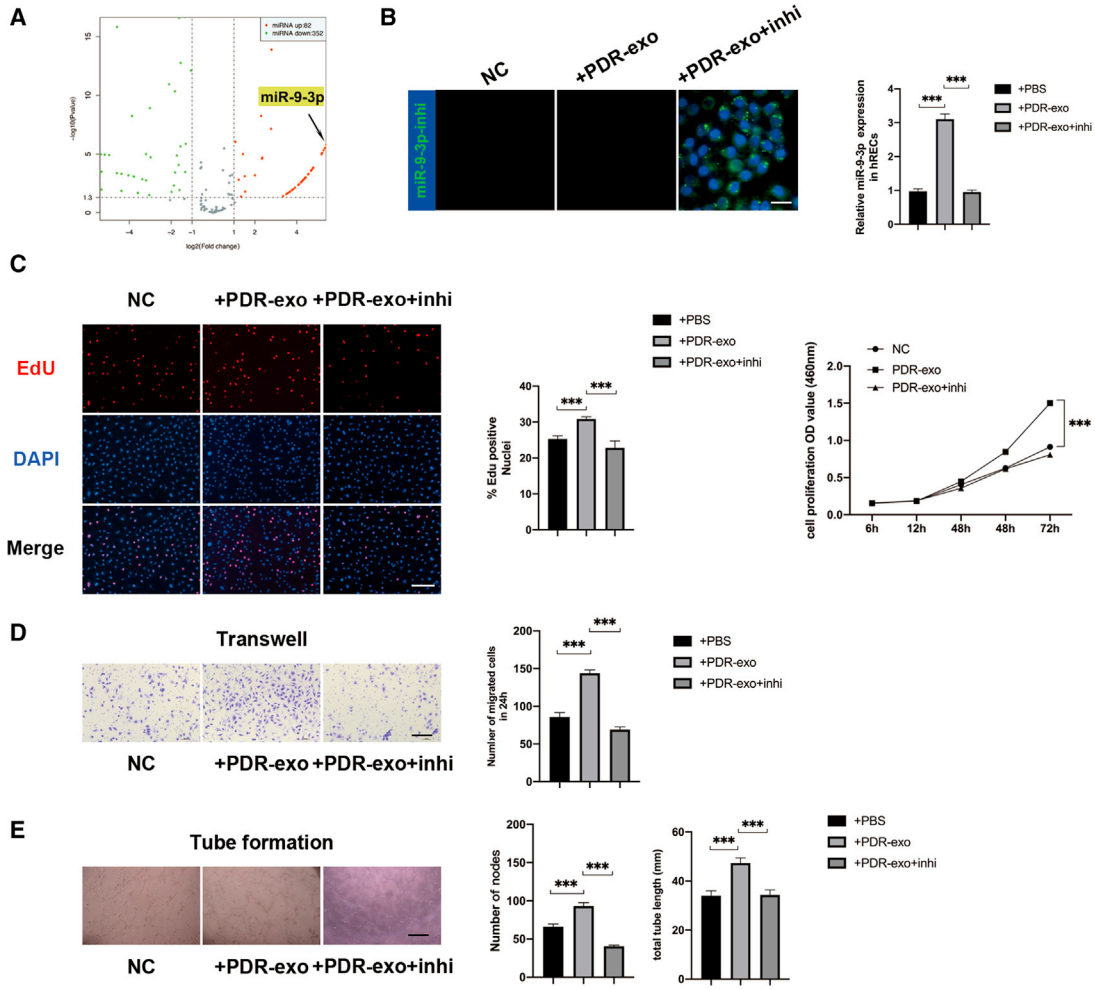

Figure 2. PDR-exo regulate vascular functions in an miR-9-3p-dependent manner

(A) Volcano plot shows dysregulated miRNAs in PDR-exo. In total, the expression levels of 82 miRNAs were upregulated and 352 miRNAs were downregulated in the PDR-exo compared with the MH-exo. (B) The FAM-labeled miR-9-3p inhibitor oligonucleotides (miR-9-3p inhi) (50 nM) were transfected into hRECs and fluorescence microscopy revealed the transfection efficiency. Scale bar, 20 μm. (C–E) miR-9-3p inhi in hRECs downregulated the enhanced cell proliferation, migration, and tube-forming ability. Scale bar, 100 μm. EdU, transwell, and tube formation assay were conducted three independent times and each group included three replicas. Three independent experiments as well as five replicas were conducted in cck8 assay. Mean ± SEM are provided and ***$p < 0.001$.

the concentration of vesicles secreted from hMGs under the two different conditions ($p > 0.05$, Figure S3B), which means that high glucose caused changes in the expression level of miR-9-3p in hMGs, rather than enhancing the secretion of the exosomes. To exclude the possibility that miR-9-3p expression may be induced by other pathological changes, we exposed four cell types to hypoxia to mimic the *in vivo* hypoxia environment of DR. A 1.5% oxygen condition for 48 h did not alter the miR-9-3p expression level in all cell types, or in secreted exosomes (Figures S3D and S3E). Also, we exposed four different retina cell types to 20 μg/mL LPS for 24 h to mimic inflammation conditions.[36–38] qRT-PCR results validated that, under inflammation conditions, the miR-9-3p expression was significantly downregulated in ARPE19-derived exosomes and was maintain at the same in the other three cell types (Figures S3F and S3G). Collectively, these results indicate that hMGs might be the main source of exosomal miR-9-3p under high glucose, which could be shuttled into hRECs to mediate vascular functions.

HGMG-exo leads to excessive vascular sprouting, whereas miR-9-3p depletion in HGMG abolishes this effect

Next, exosomes from low or high glucose cultured hMGs (LGMG-exo and HGMG-exo, respectively) were isolated and have the protein marker verified (Figure 5C). Multiple *in vitro* experiments demonstrated that cell proliferation, migration, and tube-formation ability were significantly enhanced after 100 μg/mL HGMG-exo treatment for 48 h. Of note, the miR-9-3p mimics loaded in LGMGs increased the miR-9-3p level in its derived exosomes as well as the proangiogenic effects on hRECs, while pre-inhibition of miR-9-3p in HGMGs

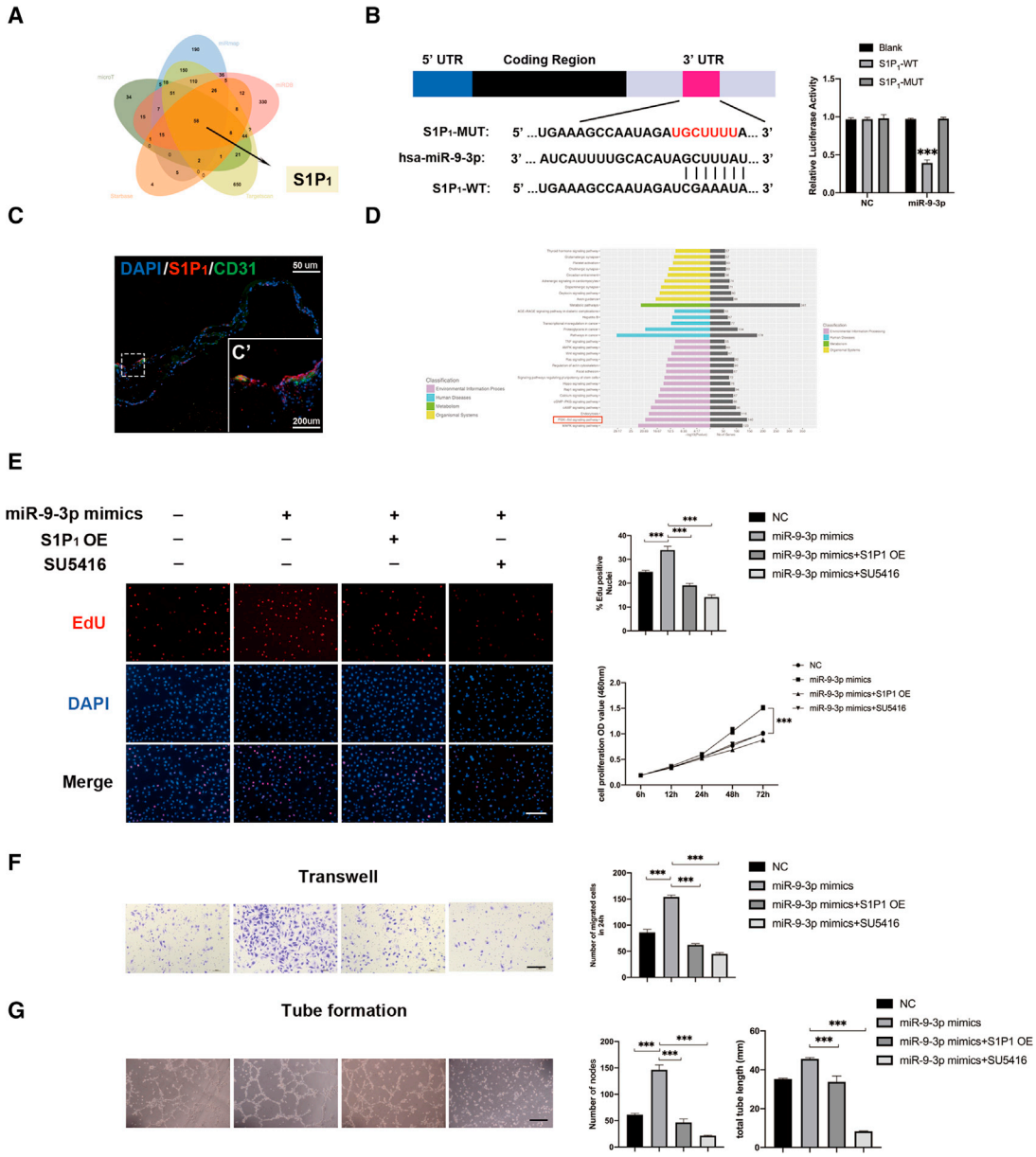

Figure 3. miR-9-3p acts as a proangiogenic factor by targeting $S1P_1$

(A) Venn diagram depicting overlap of predicted mRNAs that are regulated by miR-9-3p. (B) The putative binding sites for miR-9-3p in the 3′ UTR of $S1P_1$. Luciferase activity assay of HEK293T cells transfected with luciferase constructs containing WT-3′ UTR and MUT-3′ UTR of $S1P_1$. The experiment was repeated three times. (C) Immunostaining showing co-staining of CD31 (labeled green) with $S1P_1$ (labeled red) in the proliferative membrane. Higher magnification images are displayed in (C'). (D) Kyoto Encyclopedia of Genes and Genomes analysis revealed that AKT signaling pathway was notably activated in PDR-VH. (E–G) Effects of the miR-9-3p elevation (miR-9-3p mimics) and $S1P_1$ overexpression ($S1P_1$ OE) on (E) cell viability and proliferation, (F) migration, and (G) tube formation in hRECs. To verify that VEGF signaling is necessary for the angiogenic effects of $S1P_1$ inhibition, SU5416, a potent selective inhibitor of VEGFR, was added at a concentration of 20 μM. Scale bar, 100 μm. EdU, transwell, and tube formation were conducted three independent times and each group included three replicas. Three independent experiments as well as five replicas were conducted in cck8 assay. Mean ± SEM are provided and ***p < 0.001.

ameliorated the proangiogenic effects of HGMG-exo ($p < 0.05$, Figures 5D–5F). Collectively, the improved p-VEGFR2 protein expression, as well as its translocation from cell membranes resulting from HGMG-exo treatment, was totally blocked when miR-9-3p was pre-depleted in hMGs ($p < 0.05$, Figures 5G–5H). Taking together, our data indicate that exosomes derived from hMGs could promote angiogenesis under high glucose conditions depending on its elevated miR-9-3p expression level.

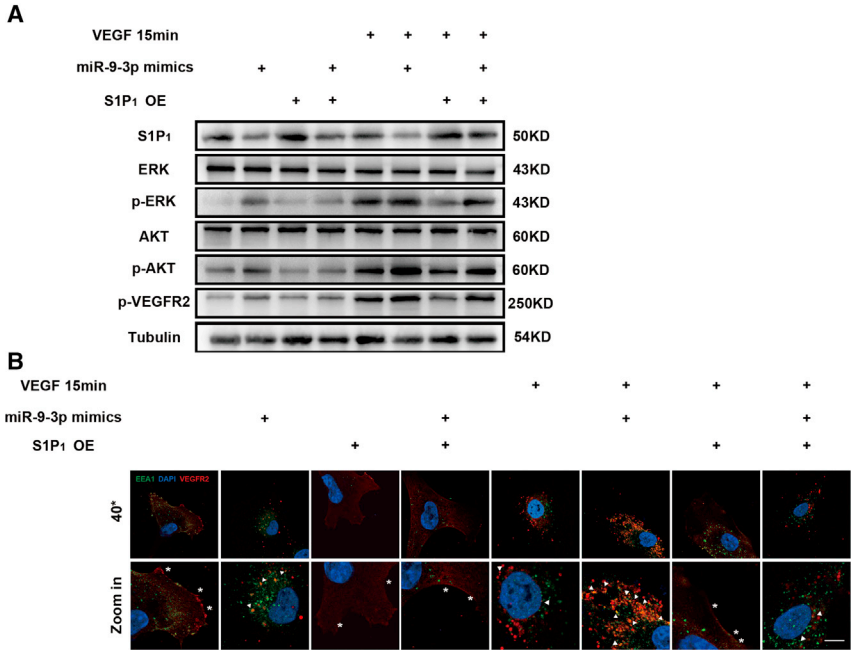

Figure 4. The MiR-9-3p/S1P$_1$ axis promotes angiogenesis by activating the VEGFR2 signaling pathway in the presence or absence of exogenous VEGF-A

(A) Endogenous VEGF-A induced phosphorylation of VEGFR2 and downstream AKT, and ERK were all inhibited by S1P$_1$ OE. After blocking autocrine VEGF-A by sFlt1, exogenous VEGF-A-induced rapid activation of VEGFR2 was also downregulated in the S1P$_1$ OE group. (B) Analysis of VEGFR2 internalization based on immunostaining assay in hRECs. HRECs transfected with miR-9-3p mimics or S1P$_1$ plasmid were processed for immunofluorescence microscopy using antibodies to VEGFR2 (labeled red) and EEA1 (labeled green). Nuclei were stained with DAPI (labeled blue). Arrows indicate the co-distribution of VEGFR2 with EEA1 (labeled green), and * indicate VEGFR2 located in cell membranes. Scale bar, 10 μm.

HGMG-derived exosomal miR-9-3p promotes angiogenesis *in vivo*

Moreover, to explore whether HGMG-exo enhances retinal angiogenesis *in vivo*, mouse MGs were primarily cultured and validated using glial cell markers (vimentin and glutamine synthesis,[39] as shown in Figure S4). Vehicle, LGMG-exo, or HGMG-exo were administered to the oxygen-induced retinopathy (OIR) mice, a well-characterized model that mimics the human pathological process of PDR (Figure 6A).[40,41] Flat-mount images showed that all OIR mice showed typical central avascular areas, while intravitreal administration of HGMG-exo significantly enhanced retinal neovascularization, as demonstrated by 50% more area of neovascularization (NV) (Figures 6B–6D). To measure proliferation in retinal endothelial cells, OIR and wild-type (WT) mice at P17 were injected with the nucleotide analog bromo-2-deoxyuridine (BrdU) 8 h before being sacrificed.[42–44] Compared with blank control (OIR-blank), vehicle control (OIR-PBS), or the PBS (+LGMG-exo)-treated group, the number of BrdU$^+$ cells/mm^2 increased after HGMG-exo treatment ($p < 0.05$). Moreover, considering that miRNA is highly conservative in mammals, we assumed that inhibition of mmu-miR-9-3p in OIR mice might rescue the abnormal retinal angiogenesis and proliferation caused by HGMG-exo. To verify this hypothesis, mmu-miR-9-3p inhibition (miR-9-3p-inhi) was intravitreally injected to OIR mice at P12 and P15. As shown in Figures 6C and 6D, miR-9-3p-inhi notably reduced retinal neovascularization as well as endothelial cell proliferation. It is worth noting that, compared with WT retina control, we did not observe significant increase in BrdU$^+$ cell number in the OIR-blank ($p = 0.480$) as well as in OIR-PBS groups ($p = 0.263$). We further examined the expression of Ki67 (proliferation marker) and PH3 (mitotic marker) by western blotting and immunofluorescence, respectively. Compared with normal control, the Ki67 protein level in endothelial cells (sorted from retina tissues using endothelial surface marker CD31) was significantly increased in OIR retinas, but no significant increase was observed in PH3 immunofluorescence ($p = 0.250$) (Figures 6E, S5A, and S5B). The immunofluorescence and western blotting results suggest that BrdU, as well as PH3, staining was underpowered to detect the elevated proliferation in the OIR model group at P17 and, compared with BrdU and PH3 staining, Ki67 detection may be a more sensitive method for quantifying endothelial proliferation.

DISCUSSION

There is an urgent need to investigate the mechanism of abnormal angiogenesis for developing new pharmaceutic interventions for DR. Multiple studies have pointed out that exosomal miRNAs may have diverse expression patterns in different disease states and play important roles in disease pathology.[21,45,46] Here, we present solid evidence that exosomes derived from the vitreous humor of PDR patients promote abnormal angiogenesis. Exosomal sequencing and *in vitro* and *in vivo* experiments revealed that retinal Müller cells modulate vascular dysfunction by secreting exosomes containing miR-9-3p, which targets the S1P$_1$/AKT/VEGFR2 pathway. This dynamic crosstalk between Müller cells and endothelial cells provides a new insight on the breaking of retinal neurovascular units and may potentially contribute to the future diagnosis and intervention of DR.

Exosomes, shed by various cell type, can exist extensively in body fluid; in the eye, they can exist in tears, aqueous humor, vitreous humor, and blood.[47,48] During the past decade, exosomes have emerged as a promising field in biomedical research as biomarkers for diagnosing diseases[19,49,50] or participants in cell-to-cell communication through receptor-ligand interactions. In ocular diseases, Ragusa et al. previously performed miRNA sequencing on vitreal exosomes from uveal melanoma patients who underwent ocular

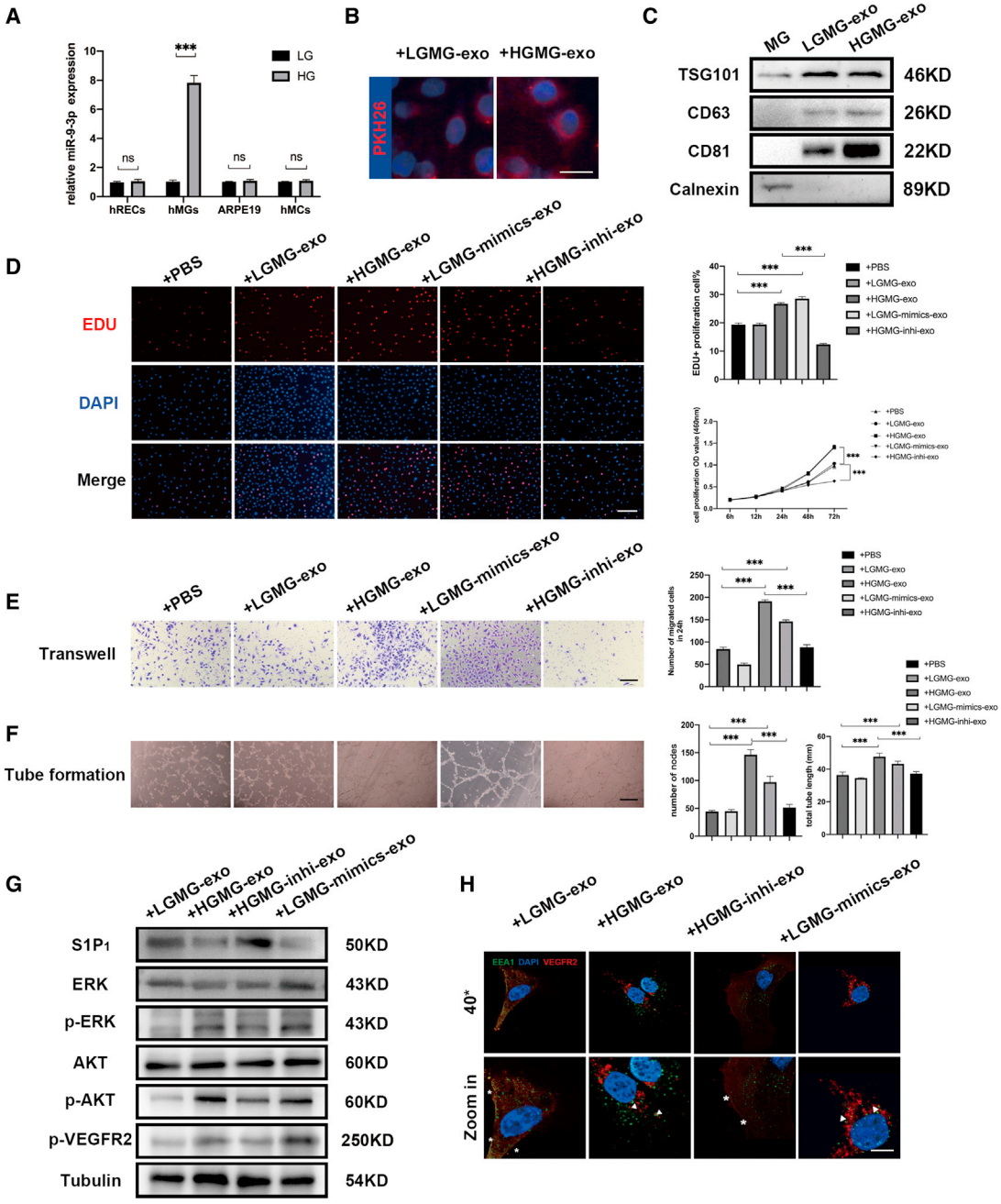

Figure 5. hMG-derived exosomal miR-9-3p/S1P$_1$ modulate hREC functions *in vitro*

(A) qRT-PCR to detect relative miR-9-3p expression in different cell types cultured in low (5.5 mM) or high glucose (30 mM) for 48 h. (B) Uptake of exosomes by hRECs was detected by PKH26. Exosomes labeled with PKH26 are stained red, while the nuclei of hRECs are stained blue. Scale bar, 20 μm. (C) Western blot bands showing exosomal surface marker protein expression levels of TSG101, CD63, CD81, and Calnexin. (D–F) Effects of the LGMG-exo and HGMG-exo on (D) cell viability and proliferation, € migration, and (F) angiogenesis in hRECs. After administration of 100 μg/mL HGMG-exo for 48 h, the cell viability, proliferation, migration, and angiogenesis capacity of hRECs were upregulated. Scale bar, 100 μm. EdU, transwell, and tube formation assay were conducted three independent times and each group included three replicas. Three independent experiments as well as five replicas were conducted in cck8 assay. Mean ± SEM are provided and ***$p < 0.001$. (G) Western blot for S1P$_1$, p-VEGFR2, and AKT/ERK-related proteins in hRECs after LGMG-exo, HGMG-exo, HGMG-inhi-exo, and LGMG-mimics-exo treatment for 48 h. (H) Analysis of VEGFR2 internalization based on immunostaining assay using antibodies to VEGFR2 (labeled red) and EEA1 (labeled green). Nuclei were stained with DAPI (labeled blue). Arrows indicate the co-distribution of VEGFR2 with EEA1 (labeled green), and * indicate VEGFR2 located in cell membranes. Scale bar, 10 μm.

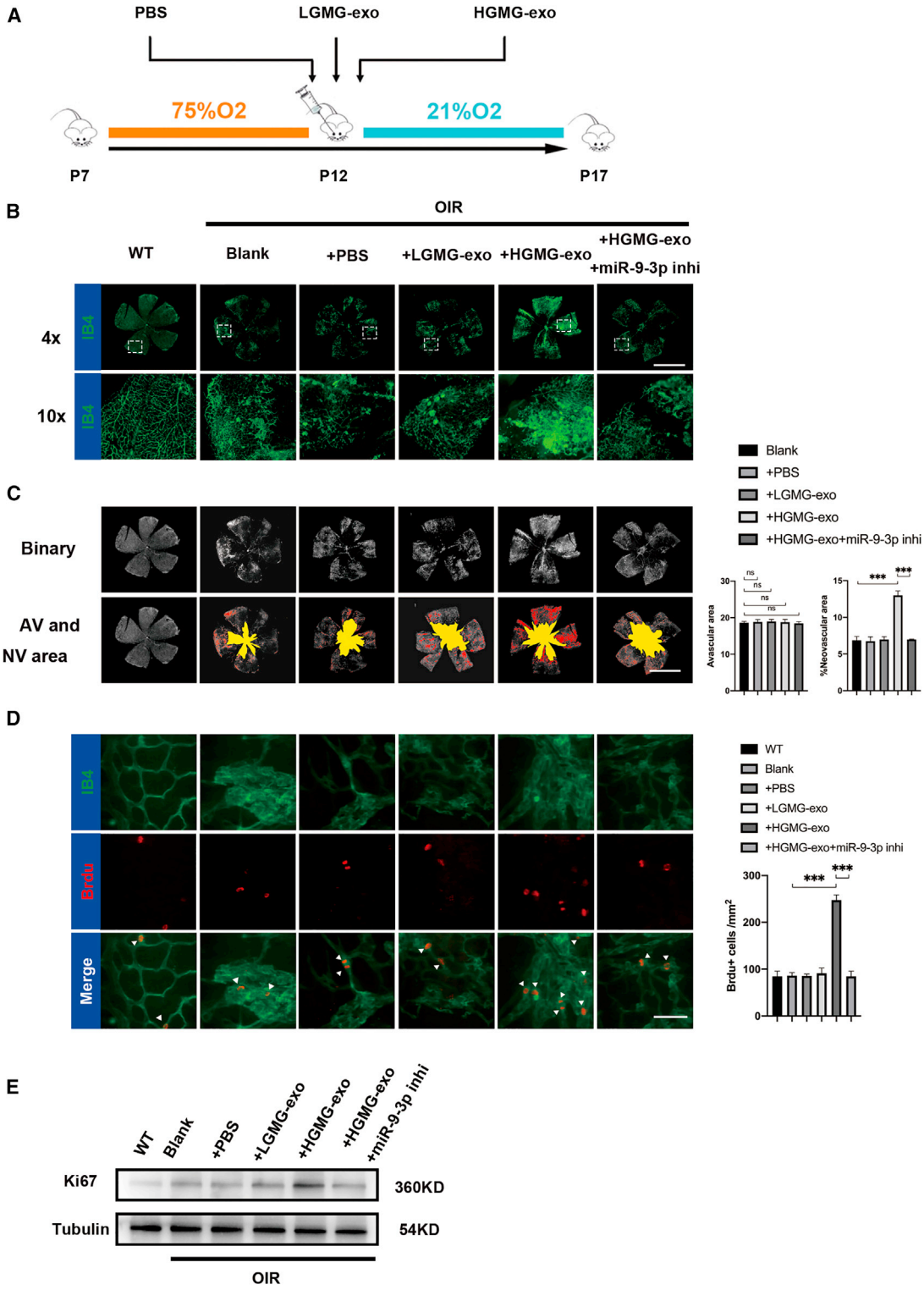

Figure 6. MG-derived exosomal miR-9-3p promote retinal angiogenesis *in vivo*

(A) Flowchart of the *in vivo* experimental design. (B and C) Retinal flat mounts of P16 C57BL/6J mice after OIR induction and intravitreal injection of 20 ng/μL LGMG-exo, HGMG-exo, or vehicle at P12 (yellow and red identify the avascular area and neovascularization, respectively). There was a significant elevation in neovascularization in the

(legend continued on next page)

enucleation.[21] However, due to the relatively small volume of human vitreous, knowledge regarding the function of exosomes in retinal diseases remains limited and at the very early stage.[51,52] The expression profiles of the miRNAs in the vitreous humor of DR patients are scarce, also because the control samples are hard to obtain due to ethical reasons. Recently, Friedrich et al. reported that miR-20a-5p, miR-23b-3p, miR-142-3p, miR-185-5p, miR-326, and miR-326-5p were remarkably elevated in PDR patients compared with non-diabetic patients with MH.[53] Interestingly, only miR-23b-3p was detected to be significantly elevated in PDR patient specimens, while the others showed no significant changes in our exosomal miRNA sequencing, indicating that these miRNAs might be secreted into the vitreous humor in an unclear manner independent of exosomes. In this study, we did not subdivide the PDR patients according to their histological or progression stages. Further study should focus on whether the expression level of exosomal miR-9-3p differs in different stages of PDR. Also, whether these biofluid miRNAs carried by exosomes could play a role in providing a more detailed characterization of the different stages of the disease requires further research.

We found that miR-9-3p was remarkably upregulated in PDR-exo based on the exosomal miRNA sequencing of the PDR-exo and MH-exo. A previous study showed that *miR-9*, upregulated in glioma specimens and cells, could significantly enhance proliferation, migration, and invasion of both glioma cells and vascular endothelial cells.[54] Also, Zhou et al. reported that, in thrombi recanalization, miR-9-5p could promote migration, invasion, and angiogenesis of endothelial progenitor cells by attenuating TRPM7 expression.[55] Our data further validate the important role of Müller cell-derived exosomal miR-9-3p in regulating vascular function in PDR. Mechanically, our results highlight that exosomal miR-9-3p upregulation of VEGFR2 phosphorylation depended on downregulation of $S1P_1$ and subsequent activation of the AKT/ERK pathway. Overexpression of $S1P_1$ as well as SU5416 neutralizes the effect of exosomal miR-9-3p in elevating cell proliferation, migration, and tube formation abilities of hRECs, indicating that the $S1P_1$ depletion as well as the activation of the AKT/ERK pathway by miR-9-3p was necessary to induce hRECs hypersprouting.

Numerous reports have pointed out that VEGF signaling, more precisely, VEGF-A-induced VEGFR2 phosphorylation, was the main regulator of neovascularization.[56,57]. In this work, we demonstrate that HGMG-exo contributes to pathological angiogenesis by mediating the endothelial reactivity toward endogenous or exogenous VEGF-A, and these effects largely depend on the downregulation of $S1P_1$ level in hRECs. Of note, it has been previously reported that $S1P_1$ depletion caused enhanced VEGF-A protein level in mouse embryos.[58] Since MGs are believed to the main source of increased VEGF-A level in vitreous humor under hypoxia and hyperglycemia,[59,60] it is reasonable to conjecture that elevated mir-9-3p level in HGMG may also influence VEGF-A secretion. Whether miR-9-3p could cause both dysregulated reactivity in hRECs and more paracrine VEGF-A production from HGMG still needs more experimental evidence for validation.

In conclusion, our study focused on understanding the intercellular communication in the retinal neurovascular unit, in particular how hMGs mediate hREC function via miRNAs loaded in exosomes. Our data highlight the role of exosomal miR-9-3p in PDR secreted by hMGs in the regulation of retinal angiogenesis by targeting the $S1P_1$/AKT/VEGFR2 pathway. Collectively, our study provides a better understanding on the exact cellular and molecular mechanisms underlying DR and sheds light on new potential therapeutic targets in future.

MATERIALS AND METHODS

Patients and tissue samples

The procedures used in this study conformed to the tenets of the Declaration of Helsinki. This study was approved by The Ethics Committee of the Faculty of Medicine, Nanjing Medical University (2017-SR-283). Informed consent was given from all the patients. To conduct exosomal sequencing, 20 mL vitreous humor from 10 PDR patients and 30 mL from 15 MH patients (as control) were collected from 2018 to 2019 at the First Affiliated Hospital of Nanjing Medical University (Table S1). All the *in vitro* experiments were conducted using vitreous humor from 65 PDR patients and 63 MH patients (Tables S2 and S3). Vitreous humor samples were harvested at the beginning of pars plana vitrectomy without infusion.

Cell culture

Multiple retinal cell types, including hRECs, hMGs, hMC3, and ARPE19 were purchased from the American Type Culture Collection. Human primary endothelial cells (hRECs) at passages 2 to 3 were used for this study and flow cytometry was conducted to verify the protein markers CD31 and CDH5. For *in vivo* experiments, primary cultures of mouse retinal MGs were conducted following the established protocol with minor modifications,[39,61,62] and had its purity validated using immunocytochemistry as shown in Figure S4. HRECs, hMGs, hMC3, and ARPE19 were cultured in DMEM (5.5 or 30 mM glucose) media contain 10% FBS and 1% pen/strep. To exclude the hyperosmolarity effects on miR-9-3p expression, hMGs were incubated in media containing normal glucose (5.5 mM glucose), high glucose (30 mM glucose), or in hyperosmolar status (5.5 mM glucose and 24.5 mM mannitol) as an osmotic control

HGMG-exo-treated group compared with the vehicle or LGMG-exo-treated groups. ***$p < 0.001$; $n = 8$. Scale bar, 1,000 μm. (D) Effects of HGMG-exo (5 μg/μL) and miR-9-3p deletion (induced by 100 nM miR-9-3p inhi) on cell proliferation as demonstrated by $BrdU^+$ cell count. Scale bar, 100 μm. Mean ± SEM are provided and ***$p < 0.001$. (E) Endothelial proliferation assessed by western blotting using Ki67 antibody. The Ki67 protein level in endothelial cells (sorted from retina tissues using endothelial surface marker CD31) was significantly increased in OIR retinas, and further upregulated in the HGMG-exo group.

(Figure S3A). To study the $S1P_1$ overexpression effects on VEGFR2 activation, hRECs were serum starved overnight and the tyrosine phosphorylation of VEGFR2 was stimulated by adding 50 ng/mL human recombinant VEGF-A (Proteintech Group, USA) for 15 min at 37°C.

Exosome isolation

Vitreous humor or conditioned cell culture supernatant was collected and centrifuged at 300 × *g* for 10 min to remove cell debris. After centrifugation at 2,000 × *g* for 10 min, the supernatant was collected and centrifuged again at 100,000 × *g* for 60 min. The pellets were collected, washed with PBS and centrifuged at 100,000 × *g* for 70 min.[63] The final pellets were resuspended in 100 μL PBS.

Microarray analysis of exosomal miRNAs

MicroRNAs (miRNAs) have been reported as the most abundant RNA species in exosomes.[64] We pooled the vitreous humor (4 mL) harvested from two PDR patients or two MH patients (as control) as one sample for exosomal sequencing analysis. In each sample, a total of 4 mL vitreous humor was mixed with RiboTM Exosome Isolation Reagent and exosome isolation was performed according to the manufacturer's instructions. Exosomal RNA was extracted using a HiPure Liquid miRNA Kit (Megan, Shanghai, China). Fifty nanograms of exosomal RNA from each of the samples were used to generate small RNA libraries using the NEBNext Multiplex Small RNA Library Prep Set for Illumina (NEB, USA) according to manufacturer's instructions. The libraries were sequenced by HiSeq 2500 (Illumina, USA) with single-end 50 bp at RiboBio (Guangzhou, China). Differentially expressed miRNAs were then identified according to the fold change, and the p value was calculated using a t test. The threshold set for the up- and downregulated genes was a fold change of ≥ 2.0 and a p value of ≤ 0.05.

Transmission electron microscopy

Isolated exosomes were immediately fixed in 4% paraformaldehyde (PFA) at 4°C for 2 h. Sections of 0.5 μm thickness were prepared under a light microscope and then ultra-thin sections of 60 nm thickness were prepared,[65] which were stained with uranium acetate and lead citrate, and observed under a transmission electron microscope (HT7700, Nanjing, China).

Uptake of exosomes by endothelial cells

PKH dye (Sigma, USA) was 1:1,000 diluted and added into 20 μg exosome suspension at 37°C for 15 min. Next, the mixed liquor was washed by PBS once and centrifuged at 100,000 × *g* for 60 min. Then PKH67-labeled exosomes were cocultured with endothelia cells for 24 h. Uptake of exosomes was observed under a confocal fluorescence microscope (MIC00223 LSM5 Live, Nanjing, China). The whole process was entirely performed in the absence of the light.

Cell transfection

hRECs at passages 2 or 3 were seeded in 12-well plates at 5×10^5 cells/well and cultured for 24 h to reach 50%–70% confluence and then transfected with mimics-nc, miR-9-3p mimics, inhibitor-nc, and miR-9-3p mimics (all purchased from RiboBio) using Lipofectamine 3000 reagent (Thermo Fisher Scientific, USA) at final levels of 50 nM according to the manufacturer's protocol for 48 h; the sequences are provided in Table S2. In a subsequent study, the hRECs were stably transfected with a control plasmid or $S1P_1$ plasmid (GenePharma, Shanghai, China). Lipofectamine 3000 reagent was used for transfection as described above.

RNA isolation and quantification and qRT-PCR

Total RNA from hRECs was extracted using Trizol reagent (Invitrogen, USA) in accordance with the manufacturer's instructions. cDNA for qRT-PCR was synthesized using a miDETECTA Track miRNA qRT-PCR Starter Kit (RiboBio) in accordance with the manufacturer's instructions. The primers for miR-9-3p and external control miR-39-3p were obtained from RiboBio. The sequences are covered by a patent.

Bioinformatics analysis

The differential miRNAs expression heatmap was constructed using the pheatmap package. The miRNAs regulating the $S1P_1$ gene were predicted using the TargetScan database (http://www.targetscan.org/), miRmap database (https://mirmap.ezlab.org/), microT database (http://diana.imis.athena-innovation.gr/DianaTools/index.php?r=site/index), Starbase database (https://starbase.sysu.edu.cn/), and the miRDB database (http://mirdb.org/). A Venn diagram was employed to obtain the intersection of the three database prediction results.

Cell proliferation assay

Cell proliferation was measured using the cck-8 kit (MCE, USA) and the EdU Cell Proliferation kit with an Alexa Fluor 596 Imaging kit (Thermo Fisher Scientific) following the manufacturer's instructions. In brief, normal hRECs or hRECs at an initial density of 5×10^3 cells/well, cocultured with 100 μg/mL MH-exo or PDR-exo, were seeded into 96-well plates and transfected with various oligonucleotides for 48 h. The cell proliferation was evaluated by 450 nm absorbance values at 6, 12, 24, 48, and 72 h thereafter using an enzyme-linked immunosorbent assay plate reader. Data are presented as mean ± SD of five replicates. Regarding the EdU assay, 100 μL 50 μM EdU medium was added into each well and incubated for 2 h in 37°C. The cells were then washed twice using PBS for 10 min, fixed in 4% PFA for 15 min, neutralized with 2 mg/mL glycine, and washed with PBS before permeabilizing with 0.5% Triton X-100 for 10 min. Finally, the hRECs were labeled using 100 μL Apollo-596 staining agent and washed in 0.5% Triton X-100 three times. EdU assay was performed three times independently and a total of three randomly selected fields were imaged in each condition using a confocal fluorescence microscope (MIC00223 LSM5 Live). The percentage of EdU-positive cells (labeled red) was calculated and analyzed using ImageJ software.

Transwell assay

Transwell assay was performed using 24-well chambers containing membrane filter inserts. After 48 h of transfection, each group of

hRECs was starved for 24 h. After 24 h of conventional culture, the transwell chamber was removed, and the cells on the inner surface of the apical chamber were removed with a cotton swab. Afterward, the cells that migrated into the lower side of the membrane were fixed with 4% PFA for 15 min, stained with 0.5% crystal violet solution for 15 min, and washed three times with PBS. Transwell assay was performed three times independently and a total of three randomly selected fields were imaged in each condition. Micrographs were acquired with a DP71 digital camera (Olympus).

Tube formation assay

Cell culture plates (96 wells) were coated with 50 μL basement membrane matrix (Matrigel; BD Biosciences, USA). HRECs were seeded at a density of 1×10^6 cells/well and treated with ECM medium for 8 h at 37°C. Capillary-like tube structures formed by hRECs on the Matrigel were photographed with a DP71 digital camera (Olympus). Tube formation was quantified by counting the total length of branching points of the capillary-like structures and calculating number of nodes per visual field. Tube formation assay was performed three times independently and a total of three randomly selected fields were imaged in each condition. Micrographs were acquired with a DP71 digital camera (Olympus).

Western blot analysis

PDR-exo or MH-exo proteins were determined using a BCA protein assay kit (Thermo Fisher Scientific) according to manufacturer's instructions. The phosphotyrosine content of the VEGFR2, as well as AKT/ERK signaling pathways, was measured as described previously using western blotting assay.[66,67] A total of 30 μg protein harvested from each group of hRECs (quantified using a BCA protein assay kit) was utilized for western blotting analysis. After blocking with 5% skim milk, membranes were incubated with antibodies against respective primary antibodies and appropriate secondary antibodies were used. Tubulin (Proteintech Group, USA) was applied as a loading control. To identify the source of the exosomes, we labeled the exosomes with different cell type markers and performed a subsequent analysis (Figure S3C). All protein bands were detected with SuperSignal West Pico Chemiluminescent Substrate (Pierce, USA) on Tanon 5200 Multi (Tanon, USA). To detect endothelial proliferation in the OIR model, endothelial cells were first sorted using endothelial surface marker CD31 (Abcam, USA) and processed for immunoblotting assay using antibodies to Ki67 (Proteintech Group). Tubulin (Proteintech Group) was applied as a loading controls.

Dual-luciferase assay

Luciferase reporter assay was performed as previously described to explore the potential regulation mechanisms of miR-9-3p.[68] Cells were cotransfected with luciferase reporter plasmid ($S1P_1$-WT, $S1P_1$-MUT) and miR-9-3p mimics (all purchased from RiboBio) in HEK293T cells. The activities of the luciferase plasmid were measured 48 h later using the Dual-Luciferase Reporter 1000 Assay System (Promega).

Experimental retinal neovascularization

Experimental retinal neovascularization was induced in C57BL/6 mice, as described previously.[40,69] Mice were exposed to 75% oxygen on postnatal day 7 (P7) and then returned to normal oxygen pressure on P12. The mice were divided into five groups as follows: (1) WT; (2) OIR mice; (3) OIR mice treated with PBS; (4) OIR mice treated with LGMG-exo (5 μg/μL); (5) OIR mice treated with HGMG-exo (5 μg/μL). To support the notion that MG-derived exosomal miR-9-3p promotes angiogenesis, rescue experiments were performed using anti-miR-9-3p in the HGMG-exo-treated group at P12 and P15.

Immunofluorescence analysis

After labeling with isolectin B4 (Vector Laboratories, USA), the retinas were cut into four or five fragments and were observed and photographed. The avascular area and the NV were calculated using ImageJ software. To evaluate the endothelial proliferation in OIR models, mouse retinas were processed for PH3 staining. In brief, retinas were collected and then permeated in 0.3% Triton X-100 overnight. Afterward, the retinas were incubated with anti-PH3 antibody (Proteintech Group).

BrdU assay

BrdU (500 μg) dissolved in sterile PBS was intraperitoneally injected to the WT or OIR mice two consecutive days before sacrifice. For BrdU labeling, retinas were denatured using 2N HCl for 1 h at room temperature, neutralized with 0.1 M Tris-HCl (pH 8.8), and then blocked in 0.3% Triton X-100 overnight. Afterward, the retinas were incubated with anti-BrdU antibody (Proteintech Group). Similarly, isolectin B4 was utilized to visualize endothelial cells here. A total of three fields were randomly selected under a confocal fluorescence microscope (MIC00223 LSM5 Live) for each condition and then the BrdU positive cells were manually counted and compared using Student's t test.

Statistical analysis

All experimental data were processed and analyzed using SPSS 21.0 (IBM, Armonk, NY, USA). Data were presented as mean ± standard deviation. Data comparisons were performed by independent sample t test with Welch correction. The Shapiro-Wilk test was used to analyze data normality. One-way analysis of variance (ANOVA) was used to compare data that were normally distributed among multiple groups. Otherwise, a non-parametric Kruskal-Wallis test was used. Cell viability at different time points were analyzed by repeated measure ANOVA. Differences were considered statistically significant when $p < 0.05$.

SUPPLEMENTAL INFORMATION

Supplemental information can be found online at https://doi.org/10.1016/j.omtn.2021.12.019.

ACKNOWLEDGMENTS

We thank colleagues from the Ethics Committee of Jiangsu Provincial People's Hospital and Jiangsu Province Hospital Core Facility Center

for their supervision. We thank medical workers in the Department of Ophthalmology in Jiangsu Provincial People's Hospital for specimen conservation. We thank the staff from the Institute of Animal Research in Nanjing Medical University for help in raising the mice. This study was supported by the National Key Research and Development Program of China (2017YFA0104100 to Q.L. and 2017YFA0104103 to S.Y.); the National Natural Science Foundation of China (81970821 to Q.L., 81900875 to Z.H., and 8207097 to P.X.); the Special-funded Program on National Key Scientific Instruments and Equipment Development (12027808 to Z.H.); the Natural Science Foundation of Jiangsu Province (BK20191059 to Z.H.); the social development program of Jiangsu Province (BE2021744 to P.X.). The funders had no role in study design, data collection and analysis, decision to publish, or preparation of the manuscript.

AUTHOR CONTRIBUTIONS

Y.L. and Q.Y. performed cell culture. Y.L., H.F., J.W., and X.L. together performed the animal experiments. Y.L. identified and verified signaling pathways. J.W. analyzed the data. Q.L., Z.H., P.X. and S.Y. provided resources and funds. Y.L. and J.W. conceived the study idea and revised the manuscript. Y.L. and Q.Y. designed the study and discussed the data. Y.L. wrote the manuscript.

DECLARATION OF INTERESTS

The authors declare no competing interests.

REFERENCES

1. GBD 2019 Blindness and Vision Impairment Collaborators; Vision Loss Expert Group of the Global Burden of Disease Study (2021). Causes of blindness and vision impairment in 2020 and trends over 30 years, and prevalence of avoidable blindness in relation to VISION 2020: the right to sight: an analysis for the Global Burden of Disease study. Lancet Glob. Health *9*, e144–e160.

2. Xu, Y., Shan, Y., Lin, X., Miao, Q., Lou, L., Wang, Y., and Ye, J. (2021). Global patterns in vision loss burden due to vitamin A deficiency from 1990 to 2017. Public Health Nutr. *24*, 5786–5794.

3. Cai, F., Jiang, H., Li, Y., Li, Q., and Yang, C. (2021). Upregulation of long non-coding RNA SNHG16 promotes diabetes-related RMEC dysfunction via activating NF-kappaB and PI3K/AKT pathways. Mol. Ther. Nucleic Acids *24*, 512–527.

4. Ye, L., Guo, H., Wang, Y., Peng, Y., Zhang, Y., Li, S., Yang, M., and Wang, L. (2021). Exosomal circEhmt1 released from hypoxia-pretreated pericytes regulates high glucose-induced microvascular dysfunction via the NFIA/NLRP3 pathway. Oxid Med. Cell Longev. *2021*, 8833098.

5. Chen, D.Y., Sun, N.H., Chen, X., Gong, J.J., Yuan, S.T., Hu, Z.Z., Lu, N.N., Korbelin, J., Fukunaga, K., Liu, Q.H., et al. (2021). Endothelium-derived semaphorin 3G attenuates ischemic retinopathy by coordinating beta-catenin-dependent vascular remodeling. J. Clin. Invest. *131*. https://doi.org/10.1172/jci135296.

6. Campochiaro, P.A., and Akhlaq, A. (2020). Sustained suppression of VEGF for treatment of retinal/choroidal vascular diseases. Prog. Retin. Eye Res. *83*, 100921.

7. Taylor, S.I., Yazdi, Z.S., and Beitelshees, A.L. (2021). Pharmacological treatment of hyperglycemia in type 2 diabetes. J. Clin. Invest. *131*. https://doi.org/10.1172/JCI142243.

8. Antoszyk, A.N., Glassman, A.R., Beaulieu, W.T., Jampol, L.M., Jhaveri, C.D., Punjabi, O.S., Salehi-Had, H., Wells, J.A., 3rd, Maguire, M.G., Stockdale, C.R., et al. (2020). Effect of intravitreous aflibercept vs vitrectomy with panretinal photocoagulation on visual acuity in patients with vitreous hemorrhage from proliferative diabetic retinopathy: a randomized clinical trial. JAMA *324*, 2383–2395.

9. Tan, G.S., Chakravarthy, U., and Wong, T.Y. (2020). Anti-VEGF therapy or vitrectomy surgery for vitreous hemorrhage from proliferative diabetic retinopathy. JAMA *324*, 2375–2377.

10. Antonetti, D.A. (2021). The neuroscience of diabetic retinopathy. Vis. Neurosci. *38*, E001.

11. Bittner, S., Ruck, T., Schuhmann, M.K., Herrmann, A.M., Moha ou Maati, H., Bobak, N., Gobel, K., Langhauser, F., Stegner, D., Ehling, P., et al. (2013). Endothelial TWIK-related potassium channel-1 (TREK1) regulates immune-cell trafficking into the CNS. Nat. Med. *19*, 1161–1165.

12. Su, E.J., Fredriksson, L., Geyer, M., Folestad, E., Cale, J., Andrae, J., Gao, Y., Pietras, K., Mann, K., Yepes, M., et al. (2008). Activation of PDGF-CC by tissue plasminogen activator impairs blood-brain barrier integrity during ischemic stroke. Nat. Med. *14*, 731–737.

13. Nian, S., Lo, A.C.Y., Mi, Y., Ren, K., and Yang, D. (2021). Neurovascular unit in diabetic retinopathy: pathophysiological roles and potential therapeutical targets. Eye Vis. (Lond) *8*, 15.

14. Yang, S., Zhang, J., and Chen, L. (2020). The cells involved in the pathological process of diabetic retinopathy. Biomed. Pharmacother. *132*, 110818.

15. Mashouri, L., Yousefi, H., Aref, A.R., Ahadi, A.M., Molaei, F., and Alahari, S.K. (2019). Exosomes: composition, biogenesis, and mechanisms in cancer metastasis and drug resistance. Mol. Cancer *18*, 75.

16. Lazaro-Ibanez, E., Faruqu, F.N., Saleh, A.F., Silva, A.M., Tzu-Wen Wang, J., Rak, J., Al-Jamal, K.T., and Dekker, N. (2021). Selection of fluorescent, bioluminescent, and radioactive tracers to accurately reflect extracellular vesicle biodistribution in vivo. ACS Nano *15*, 3212–3227.

17. Teng, F., and Fussenegger, M. (2020). Shedding light on extracellular vesicle biogenesis and bioengineering. Adv. Sci. (Weinh.) *8*, 2003505.

18. Thery, C., Witwer, K.W., Aikawa, E., Alcaraz, M.J., Anderson, J.D., Andriantsitohaina, R., Antoniou, A., Arab, T., Archer, F., Atkin-Smith, G.K., et al. (2018). Minimal information for studies of extracellular vesicles 2018 (MISEV2018): a position statement of the International Society for Extracellular Vesicles and update of the MISEV2014 guidelines. J. Extracell. Vesicles *7*, 1535750.

19. Kalluri, R., and LeBleu, V.S. (2020). The biology, function, and biomedical applications of exosomes. Science *367*. https://doi.org/10.1126/science.aau6977.

20. Li, X., Wang, J., Qian, H., Wu, Y., Zhang, Z., Hu, Z., and Xie, P. (2021). Serum exosomal circular RNA expression profile and regulative role in proliferative diabetic retinopathy. Front. Genet. *12*, 719312.

21. Ragusa, M., Barbagallo, C., Statello, L., Caltabiano, R., Russo, A., Puzzo, L., Avitabile, T., Longo, A., Toro, M.D., Barbagallo, D., et al. (2015). miRNA profiling in vitreous humor, vitreal exosomes and serum from uveal melanoma patients: pathological and diagnostic implications. Cancer Biol. Ther. *16*, 1387–1396.

22. Pegtel, D.M., and Gould, S.J. (2019). Exosomes. Annu. Rev. Biochem. *88*, 487–514.

23. Buschmann, D., Mussack, V., and Byrd, J.B. (2021). Separation, characterization, and standardization of extracellular vesicles for drug delivery applications. Adv. Drug Deliv. Rev. *174*, 348–368.

24. Zhang, J., Chintalgattu, V., Shih, T., Ai, D., Xia, Y., and Khakoo, A.Y. (2011). MicroRNA-9 is an activation-induced regulator of PDGFR-beta expression in cardiomyocytes. J. Mol. Cell Cardiol. *51*, 337–346.

25. Ma, L., Young, J., Prabhala, H., Pan, E., Mestdagh, P., Muth, D., Teruya-Feldstein, J., Reinhardt, F., Onder, T.T., Valastyan, S., et al. (2010). miR-9, a MYC/MYCN-activated microRNA, regulates E-cadherin and cancer metastasis. Nat. Cell Biol. *12*, 247–256.

26. Qu, J., Lu, D., Guo, H., Miao, W., Wu, G., and Zhou, M. (2016). MicroRNA-9 regulates osteoblast differentiation and angiogenesis via the AMPK signaling pathway. Mol. Cell Biochem. *411*, 23–33.

27. Qian, D., Song, G., Ma, Z., Wang, G., Jin, L., Hu, M., Song, Z., and Wang, X. (2018). MicroRNA-9 modified bone marrow-derived mesenchymal stem cells (BMSCs) repair severe acute pancreatitis (SAP) via inducing angiogenesis in rats. Stem Cell Res. Ther. *9*, 282.

28. McFadyen, W.D., Sotirellis, N., Denny, W.A., and Wakelin, L.P. (1990). The interaction of substituted and rigidly linked diquinolines with DNA. Biochim. Biophys. Acta *1048*, 50–58.

29. Cartier, A., Leigh, T., Liu, C.H., and Hla, T. (2020). Endothelial sphingosine 1-phosphate receptors promote vascular normalization and antitumor therapy. Proc. Natl. Acad. Sci. U S A *117*, 3157–3166.

30. Fong, T.A., Shawver, L.K., Sun, L., Tang, C., App, H., Powell, T.J., Kim, Y.H., Schreck, R., Wang, X., Risau, W., et al. (1999). SU5416 is a potent and selective inhibitor of the vascular endothelial growth factor receptor (Flk-1/KDR) that inhibits tyrosine kinase catalysis, tumor vascularization, and growth of multiple tumor types. Cancer Res. *59*, 99–106.

31. Gaengel, K., Niaudet, C., Hagikura, K., Lavina, B., Muhl, L., Hofmann, J.J., Ebarasi, L., Nystrom, S., Rymo, S., Chen, L.L., et al. (2012). The sphingosine-1-phosphate receptor S1PR1 restricts sprouting angiogenesis by regulating the interplay between VE-cadherin and VEGFR2. Dev. Cell *23*, 587–599.

32. Fan, X., Muruganandan, S., Shallie, P.D., Dhal, S., Petitt, M., and Nayak, N.R. (2021). VEGF maintains maternal vascular space homeostasis in the mouse placenta through modulation of trophoblast giant cell functions. Biomolecules *11*, 1062. https://doi.org/10.3390/biom11071062.

33. Smith, G.A., Fearnley, G.W., Abdul-Zani, I., Wheatcroft, S.B., Tomlinson, D.C., Harrison, M.A., and Ponnambalam, S. (2016). VEGFR2 trafficking, signaling and proteolysis is regulated by the ubiquitin isopeptidase USP8. Traffic *17*, 53–65.

34. Smith, G.A., Fearnley, G.W., Abdul-Zani, I., Wheatcroft, S.B., Tomlinson, D.C., Harrison, M.A., and Ponnambalam, S. (2017). Ubiquitination of basal VEGFR2 regulates signal transduction and endothelial function. Biol. Open *6*, 1404–1415.

35. Bayliss, A.L., Sundararaman, A., Granet, C., and Mellor, H. (2020). Raftlin is recruited by neuropilin-1 to the activated VEGFR2 complex to control proangiogenic signaling. Angiogenesis *23*, 371–383.

36. He, C., Liu, Y., Huang, Z., Yang, Z., Zhou, T., Liu, S., Hao, Z., Wang, J., Feng, Q., Liu, Y., et al. (2021). A specific RIP3(+) subpopulation of microglia promotes retinopathy through a hypoxia-triggered necroptotic mechanism. Proc. Natl. Acad. Sci. U S A *118*. https://doi.org/10.1073/pnas.2023290118.

37. Fernandez-Robredo, P., Gonzalez-Zamora, J., Recalde, S., Bilbao-Malave, V., Bezunartea, J., Hernandez, M., and Garcia-Layana, A. (2020). Vitamin D protects against oxidative stress and inflammation in human retinal cells. Antioxidants (Basel) *9*. https://doi.org/10.3390/antiox9090838.

38. Kokona, D., Ebneter, A., Escher, P., and Zinkernagel, M.S. (2018). Colony-stimulating factor 1 receptor inhibition prevents disruption of the blood-retina barrier during chronic inflammation. J. Neuroinflammation *15*, 340.

39. Lopez-Colome, A.M., and Romo-de-Vivar, M. (1991). Excitatory amino acid receptors in primary cultures of glial cells from the retina. Glia *4*, 431–439.

40. Matsuda, K., Okamoto, N., Kondo, M., Arkwright, P.D., Karasawa, K., Ishizaka, S., Yokota, S., Matsuda, A., Jung, K., Oida, K., et al. (2017). Mast cell hyperactivity underpins the development of oxygen-induced retinopathy. J. Clin. Invest. *127*, 3987–4000.

41. Huang, B., Deora, A.B., He, K.L., Chen, K., Sui, G., Jacovina, A.T., Almeida, D., Hong, P., Burgman, P., and Hajjar, K.A. (2011). Hypoxia-inducible factor-1 drives annexin A2 system-mediated perivascular fibrin clearance in oxygen-induced retinopathy in mice. Blood *118*, 2918–2929.

42. Kee, N., Teixeira, C.M., Wang, A.H., and Frankland, P.W. (2007). Imaging activation of adult-generated granule cells in spatial memory. Nat. Protoc. *2*, 3033–3044.

43. Wojtowicz, J.M., and Kee, N. (2006). BrdU assay for neurogenesis in rodents. Nat. Protoc. *1*, 1399–1405.

44. Pitulescu, M.E., Schmidt, I., Benedito, R., and Adams, R.H. (2010). Inducible gene targeting in the neonatal vasculature and analysis of retinal angiogenesis in mice. Nat. Protoc. *5*, 1518–1534.

45. Takayama, K., Kaneko, H., Hwang, S.J., Ye, F., Higuchi, A., Tsunekawa, T., Matsuura, T., Iwase, T., Asami, T., Ito, Y., et al. (2016). Increased ocular levels of microRNA-148a in cases of retinal detachment promote epithelial-mesenchymal transition. Invest. Ophthalmol. Vis. Sci. *57*, 2699–2705.

46. Russo, A., Ragusa, M., Barbagallo, C., Longo, A., Avitabile, T., Uva, M.G., Bonfiglio, V., Toro, M.D., Caltabiano, R., Mariotti, C., et al. (2017). miRNAs in the vitreous humor of patients affected by idiopathic epiretinal membrane and macular hole. PLoS One *12*, e0174297.

47. Zhang, Z., Mugisha, A., Fransisca, S., Liu, Q., Xie, P., and Hu, Z. (2021). Emerging role of exosomes in retinal diseases. Front Cell Dev. Biol. *9*, 643680.

48. Klingeborn, M., Skiba, N.P., Stamer, W.D., and Bowes Rickman, C. (2019). Isolation of retinal exosome biomarkers from blood by targeted immunocapture. Adv. Exp. Med. Biol. *1185*, 21–25.

49. Colombo, M., Raposo, G., and Thery, C. (2014). Biogenesis, secretion, and intercellular interactions of exosomes and other extracellular vesicles. Annu. Rev. Cell Dev. Biol. *30*, 255–289.

50. Huang, H. (2020). Pericyte-endothelial interactions in the retinal microvasculature. Int. J. Mol. Sci. *21*. https://doi.org/10.3390/ijms21197413.

51. Wang, Y., Tang, Z., and Gu, P. (2020). Stem/progenitor cell-based transplantation for retinal degeneration: a review of clinical trials. Cell Death Dis. *11*, 793.

52. Zhang, W., Wang, Y., and Kong, Y. (2019). Exosomes derived from mesenchymal stem cells modulate miR-126 to ameliorate hyperglycemia-induced retinal inflammation via targeting HMGB1. Invest. Ophthalmol. Vis. Sci. *60*, 294–303.

53. Friedrich, J., Steel, D.H.W., Schlingemann, R.O., Koss, M.J., Hammes, H.P., Krenning, G., and Klaassen, I. (2020). microRNA expression profile in the vitreous of proliferative diabetic retinopathy patients and differences from patients treated with anti-VEGF therapy. Transl. Vis. Sci. Technol. *9*, 16.

54. Chen, X., Yang, F., Zhang, T., Wang, W., Xi, W., Li, Y., Zhang, D., Huo, Y., Zhang, J., Yang, A., et al. (2019). MiR-9 promotes tumorigenesis and angiogenesis and is activated by MYC and OCT4 in human glioma. J. Exp. Clin. Cancer Res. *38*, 99.

55. Zhou, D.M., Sun, L.L., Zhu, J., Chen, B., Li, X.Q., and Li, W.D. (2020). MiR-9 promotes angiogenesis of endothelial progenitor cell to facilitate thrombi recanalization via targeting TRPM7 through PI3K/Akt/autophagy pathway. J. Cell Mol. Med. *24*, 4624–4632.

56. Stitt, A.W., Curtis, T.M., Chen, M., Medina, R.J., McKay, G.J., Jenkins, A., Gardiner, T.A., Lyons, T.J., Hammes, H.P., Simo, R., et al. (2016). The progress in understanding and treatment of diabetic retinopathy. Prog. Retin. Eye Res. *51*, 156–186.

57. Wirostko, B., Wong, T.Y., and Simo, R. (2008). Vascular endothelial growth factor and diabetic complications. Prog. Retin. Eye Res. *27*, 608–621.

58. Chae, S.S., Paik, J.H., Allende, M.L., Proia, R.L., and Hla, T. (2004). Regulation of limb development by the sphingosine 1-phosphate receptor S1p1/EDG-1 occurs via the hypoxia/VEGF axis. Dev. Biol. *268*, 441–447.

59. Eichler, W., Kuhrt, H., Hoffmann, S., Wiedemann, P., and Reichenbach, A. (2000). VEGF release by retinal glia depends on both oxygen and glucose supply. Neuroreport *11*, 3533–3537.

60. Pannicke, T., Iandiev, I., Wurm, A., Uckermann, O., vom Hagen, F., Reichenbach, A., Wiedemann, P., Hammes, H.P., and Bringmann, A. (2006). Diabetes alters osmotic swelling characteristics and membrane conductance of glial cells in rat retina. Diabetes *55*, 633–639.

61. Hicks, D., and Courtois, Y. (1990). The growth and behaviour of rat retinal Muller cells in vitro. 1. An improved method for isolation and culture. Exp. Eye Res. *51*, 119–129.

62. Li, Y.C., Hayes, S., and Young, A.P. (1997). Steroid hormone receptors activate transcription in glial cells of intact retina but not in primary cultures of retinal glial cells. J. Mol. Neurosci. *8*, 145–158.

63. Alzhrani, G.N., Alanazi, S.T., Alsharif, S.Y., Albalawi, A.M., Alsharif, A.A., Abdel-Maksoud, M.S., et al. (2021). Exosomes: isolation, characterization, and biomedical applications. Cell Biol. Int. *13*, 152. https://doi.org/10.1002/cbin.11620.

64. Wooff, Y., Cioanca, A.V., Chu-Tan, J.A., Aggio-Bruce, R., Schumann, U., and Natoli, R. (2020). Small-medium extracellular vesicles and their miRNA cargo in retinal health and degeneration: mediators of homeostasis, and vehicles for targeted gene therapy. Front. Cell Neurosci. *14*, 160.

65. Szatanek, R., Baj-Krzyworzeka, M., Zimoch, J., Lekka, M., Siedlar, M., and Baran, J. (2017). The methods of choice for extracellular vesicles (EVs) characterization. Int. J. Mol. Sci. *18*. https://doi.org/10.3390/ijms18061153.

66. Lee, J., Jr., Chen, C.H., Chen, Y.H., Huang, M.J., Huang, J., Hung, J.S., Chen, M.T., and Huang, M.C. (2013). COSMC is overexpressed in proliferating infantile hemangioma and enhances endothelial cell growth via VEGFR2. PLoS One *8*, e56211.

67. Kofler, N., Corti, F., Rivera-Molina, F., Deng, Y., Toomre, D., and Simons, M. (2018). The Rab-effector protein RABEP2 regulates endosomal trafficking to mediate vascular endothelial growth factor receptor-2 (VEGFR2)-dependent signaling. J. Biol. Chem. *293*, 4805–4817.

68. Yoo, J.K., Lee, J.M., Kang, S.H., Jeon, S.H., Kim, C.M., Oh, S.H., Kim, C.H., Kim, N.K., and Kim, J.K. (2019). The novel microRNA hsa-miR-CHA1 regulates cell proliferation and apoptosis in human lung cancer by targeting XIAP. Lung Cancer *132*, 99–106.

69. Kim, J., Lee, Y.M., Jung, W., Park, S.B., Kim, C.S., and Kim, J.S. (2018). *Aster koraiensis* extract and chlorogenic acid inhibit retinal angiogenesis in a mouse model of oxygen-induced retinopathy. Evid. Based Complement Alternat. Med. *2018*, 6402650.

OMTN, Volume *27*

Supplemental information

Müller glia-derived exosomal miR-9-3p promotes angiogenesis by restricting sphingosine-1-phosphate receptor $S1P_1$ in diabetic retinopathy

Yu Liu, Qin Yang, Haixin Fu, Jingfan Wang, Songtao Yuan, Xinsheng Li, Ping Xie, Zizhong Hu, and Qinghuai Liu

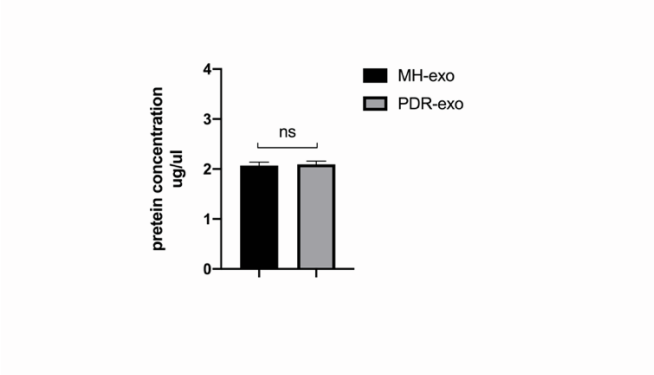

Supplementary Figure 1 Quantitation of protein level of MH-exo and PDR-exo

BCA results determined that nonsignificant difference was found in concentration of proteins level of MH-exo and PDR-exo ($p>0.05$).

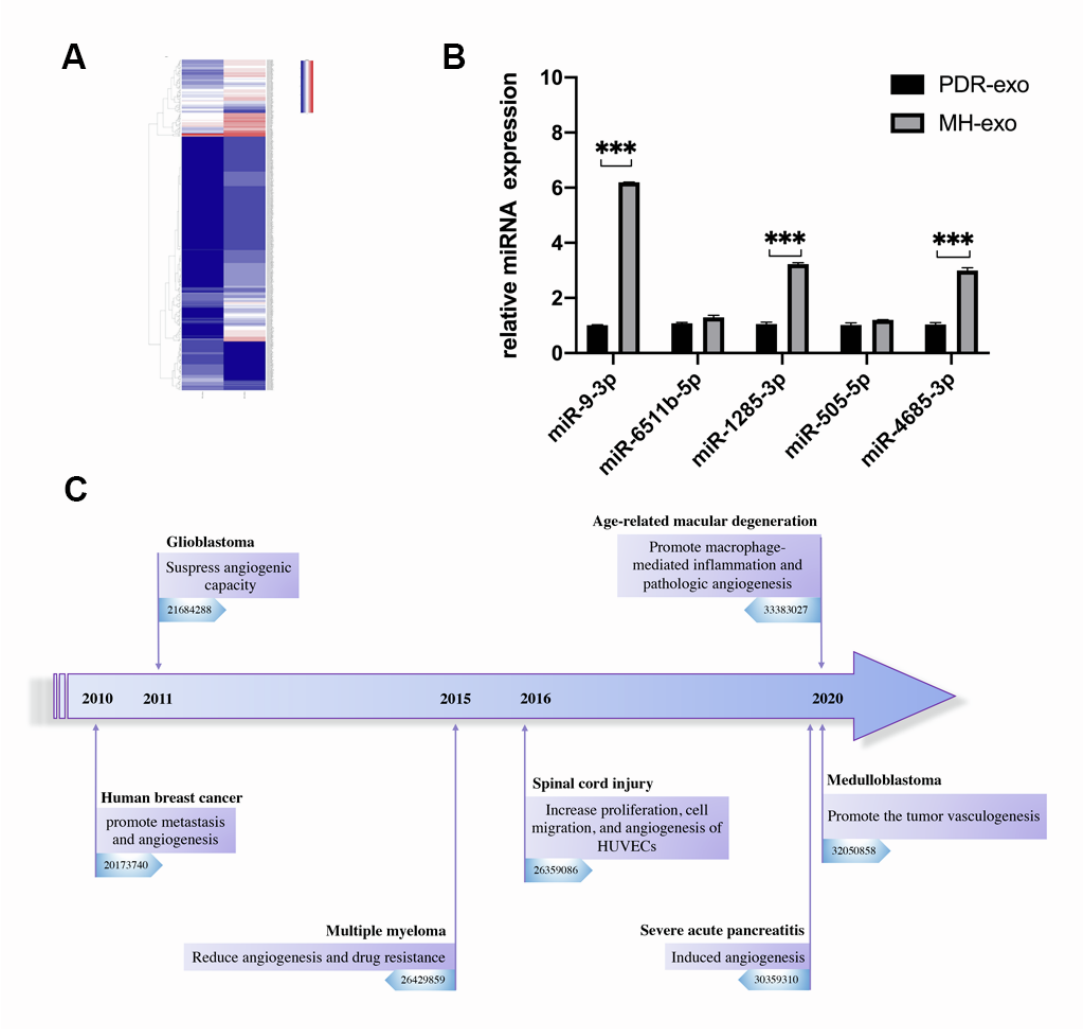

Supplementary Figure 2 Exosomal miR-9-3p was markably upregulated in the vitreous humor of PDR

(A) Heat map indicated that 82 miRNAs were up-regulated and 352 miRNAs were downregulated in the PDR-exo compared with the MH-exo. (B) RT-qPCR validated the expression level of top 5 upregulated exosomal miRNAs in the vitreous humor of PDR compared to MH patients. ***p<0.001, n=3. (C) Timeline highlighting the advances in miR-9-3p. From being reported to promote angiogenesis in human breast cancer in 2010, there has been advances on the physical characteristics and biofunction of miR-9-3p in multiple diseases.

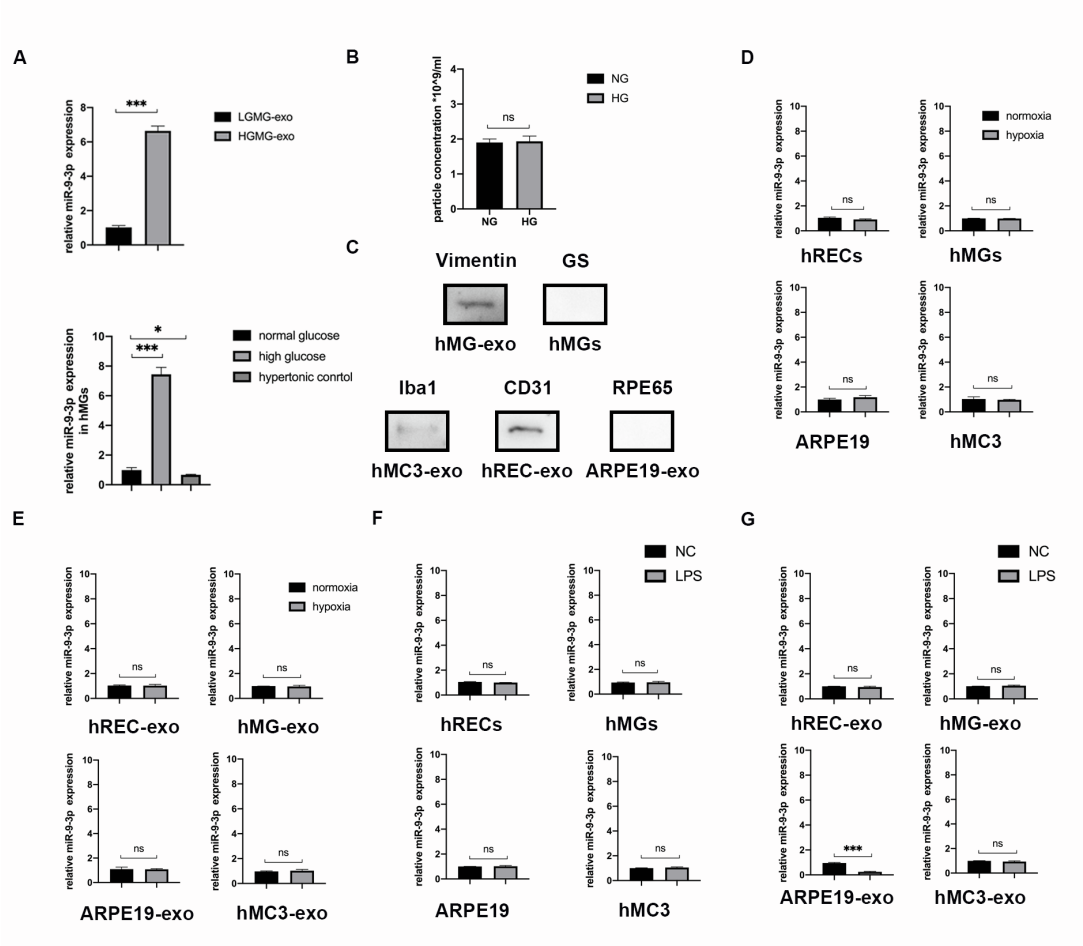

Supplementary Figure 3 Expression pattern of miR-9-3p in multiple retinal cell types

(A) Upper panel: RT-qPCR results validated that the expression level of miR-9-3p was higher in HGMG-exo than in LGMG-exo. Lower panel: Hyperosmolar status induced by 5.5 mM glucose and 24.5 mM mannitol did not alter the expression level of miR-9-3p in hMGs. (B) Nanoparticle tracking analysis confirmed that there was no difference between the particle concentration of vesicles secreted from hMGs under low (5.5mM) and high glucose (30mM). (C) Specific cell marker in cell derived exosomes as detected by western blot. Vimentin and Glutamine synthesis in müller cell derived exosomes, IBa1 in human microglial hMC3 cell derived exosomes, CD31 in endothelial cell in hRECs derived exosomes, and RPE65 in ARPE19 derived exosomes was detected. (D)-

(E) The miR-9-3p expression in four cell types or cell derived exosomes under hypoxia environment (1.5% O_2). (F)-(G) Under inflammation condition, the miR-9-3p expression was significantly downregulated in ARPE19 derived exosomes and maintain the same in the other three cell types. ***p<0.001.

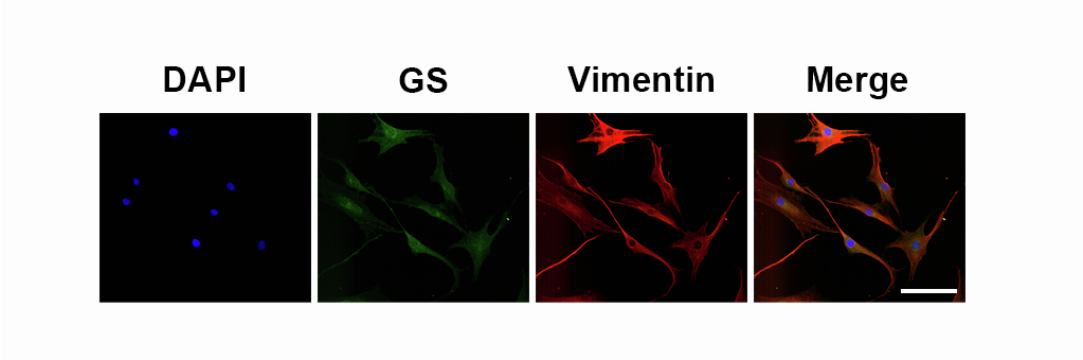

Supplementary Figure 4 Validation of primarily cultured mMGs at passage 1

Immunocytochemistry confirmed that expressions of vimentin and glutamine synthetase (GS) in MG. Scale bar = 20 μm.

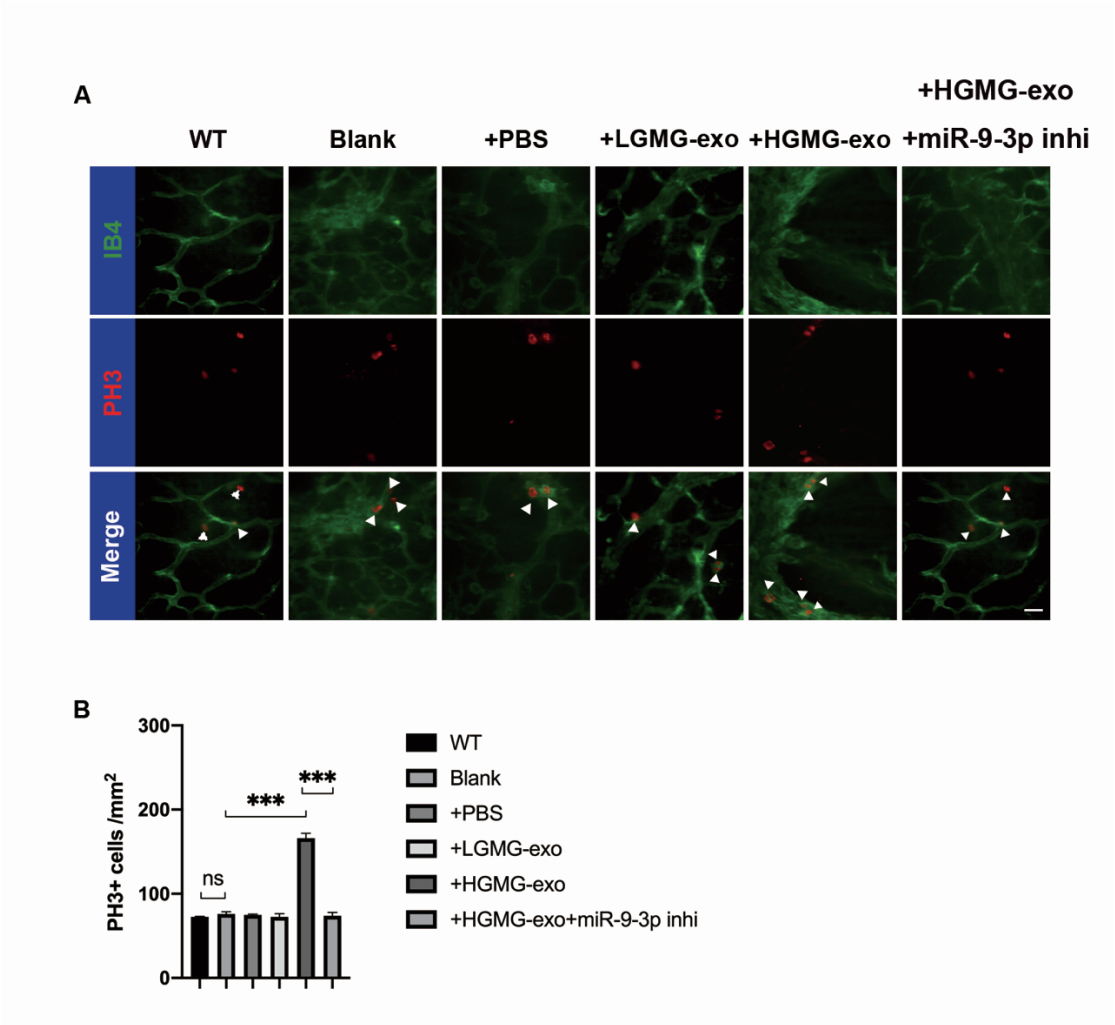

Supplementary Figure 5 PH3 immunofluorescence is underpowered to detect endothelial proliferation in OIR model

(A)-(B) Compared with normal control, no significant increase was observed in OIR-blank or OIR-PBS group using PH3 immunofluorescence ($p>0.05$)

Supplementary Table 1 Vitreous spicemen was harvested for exosomal sequencing from 10 PDR patients and 15 sex-age matched MH patients

	Sex	Age (Years)	Volume of collected vitreous humor	Operation type
PDR1	Male	58	2ml	pars plana vitrectomy
PDR2	Female	37	2ml	pars plana vitrectomy
PDR3	Female	48	2ml	pars plana vitrectomy
PDR4	Male	51	2ml	pars plana vitrectomy
PDR5	Female	61	2ml	pars plana vitrectomy
PDR6	Male	58	2ml	pars plana vitrectomy
PDR7	Male	62	2ml	pars plana vitrectomy
PDR8	Female	61	2ml	pars plana vitrectomy
PDR9	Male	59	2ml	pars plana vitrectomy
PDR10	Female	63	2ml	pars plana vitrectomy
MH1	Male	51	2ml	pars plana vitrectomy
MH2	Female	63	2ml	pars plana vitrectomy
MH3	Female	64	2ml	pars plana vitrectomy
MH4	Male	65	2ml	pars plana vitrectomy
MH5	Male	61	2ml	pars plana vitrectomy
MH6	Female	57	2ml	pars plana vitrectomy
MH7	Male	46	2ml	pars plana vitrectomy
MH8	Male	61	2ml	pars plana vitrectomy
MH9	Female	55	2ml	pars plana vitrectomy
MH10	Male	51	2ml	pars plana vitrectomy
MH11	Male	61	2ml	pars plana vitrectomy
MH12	Male	60	2ml	pars plana vitrectomy
MH13	Female	49	2ml	pars plana vitrectomy
MH14	Male	60	2ml	pars plana vitrectomy
MH15	Female	62	2ml	pars plana vitrectomy

Supplementary Table 2 Clinic features of 65 PDR patients and 63 sex-age matched MH patients.

Characteristic	Number	
	PDR	MH
Age (Years)		
45-49	**10**	**11**
50-54	**18**	**18**
55-59	**22**	**20**
60-65	**15**	**14**
Gender		
Male	**32**	**33**
Female	**33**	**30**

Supplementary Table 3 Total exosomal protein collected from PDR and MH patients

	Replica 1		Replica 2		Replica 3	
Characteristics	**PDR**	**MH**	**PDR**	**MH**	**PDR**	**MH**
Number	**21**	**21**	**21**	**21**	**23**	**21**
Volume (ml)	**42**	**42**	**42**	**42**	**46**	**42**
Total exosomal protein (ug)	**60.0**	**59.7**	**61.9**	**60.8**	**67.2**	**60.6**

Supplementary Table 4 RNA sequence of miR-9-3p mimic, inhibitor, mimic nc and inhibitor nc

Oligonucleotide	Forward	Rerverse
miR-9-3p mimic	AUAAAGCUAGAUAACCGAAAGU	ACUUUCGGUUAUCUAGCUUUAU
miR-9-3p inhibitor	ACUUUCGGUUAUCUAGCUUUAU	CAGUACUUUUGUGUAGUACAAA
Mimic-nc	UUUGUACUACACAAAAGUACUG	
Inhi-nc	CAGUACUUUUGUGUAGUACAAA	